available at www.sciencedirect.com
journal homepage: www.europeanurology.com

European Association of Urology

Surgery in Motion

Three-dimensional Virtual Models of the Kidney with Colored Perfusion Regions: A New Algorithm-based Tool for Optimizing the Clamping Strategy During Robot-assisted Partial Nephrectomy

Daniele Amparore [a,*,†], *Federico Piramide* [a,†], *Enrico Checcucci* [b], *Paolo Verri* [a], *Sabrina De Cillis* [a], *Alberto Piana* [a], *Gabriele Volpi* [a], *Giovanni Busacca* [a], *Marco Colombo* [a], *Cristian Fiori* [a,‡], *Francesco Porpiglia* [a,‡]

[a] *Division of Urology, Department of Oncology, School of Medicine, University of Turin, San Luigi Hospital, Orbassano, Italy;* [b] *Department of Surgery, Candiolo Cancer Institute FPO-IRCCS, Candiolo, Italy*

Article info

Article history:
Accepted April 4, 2023

Associate Editor:
Alexandre Mottrie

Keywords:
Three-dimensional imaging
Robotic surgery
Renal cell carcinoma
Kidney cancer
Nephron-sparing surgery
Surgical anatomy

Abstract

Background: An empirical selective clamping strategy based on the direction of the arterial branches can lead to failures during partial nephrectomy, even when assisted by three-dimensional virtual models (3DVMs).
Objective: To develop and test new 3DVMs that include kidney perfusion regions and evaluate their intraoperative accuracy in guiding selective clamping and their impact on postoperative renal function.
Design, setting, and participants: For patients with a kidney suitable for nephron-sparing surgery, 3DVMs were supplemented with a Voronoi diagram, a Euclidean distance–based mathematical tool, to calculate vascular-dominant regions the kidney.
Surgical procedure: Robot-assisted partial nephrectomy guided by perfusion-region (PR)-3DVMs.
Measurements: All anatomic information given by the PR-3DVMs was collected. Selective or superselective clamping was planned and performed intraoperatively when feasible under 3DVM assistance. Changes in split renal function (SRF) and estimated renal plasmatic flow (ERPF) were evaluated for 51 patients who underwent baseline and 3-mo postoperative renal scintigraphy.
Results and limitations: A total of 103 patients were prospectively enrolled. The median number of kidney and tumor perfusion regions were 8 (interquartile range [IQR] 7–10) and 3 (IQR 2–3), respectively. A clampless, selective clamping, and global clamping strategy was applied in eight (7.8%), 79 (76.6%), and 16 (15.5%) cases, respectively, with no differences between planning and surgery in terms of the number or order of arteries clamped or the perfusion regions that underwent ischemia. Among the 51 patients who underwent renal scintigraphy, the mean SRF decreased by 11.3%, 7.7%, and 1.7% after global, selective, and superselective clamping, respectively (p = 0.004). Similar

† These authors contributed equally to this work.
‡ These authors contributed equally to senior authorship.
* Corresponding author. Department of Urology, San Luigi Gonzaga Hospital, University of Turin, Orbassano, Turin, Italy. Tel. +39 3333352758; Fax: +39 011 9026244.
E-mail address: danieleamparore@hotmail.it (D. Amparore).

https://doi.org/10.1016/j.eururo.2023.04.005

results were obtained for ERPF (18.9%, 9.9%, and 6.0%; p = 0.02). The main limitation is the need for a bioengineer to manually refine the 3DVMs.
Conclusions: Use of mathematical algorithms for 3DVMs allows precise estimation of kidney perfusion regions to maximize the efficacy of selective clamping and minimize renal function impairment.
Patient summary: Three-dimensional models that include regions of blood flow to the kidney can be used to guide clamping of blood vessels when part of the kidney is being surgically removed. More limited clamping can reduce damage to the remaining portion of the kidney and result in better recovery of kidney function after surgery.

1. Introduction

Selective clamping of renal artery branches has been introduced as a vascular management strategy during nephron-sparing surgery (NSS) [1–5]. The rationale is to reduce the volume of renal parenchyma exposed to ischemic damage with the aim of optimizing postoperative functional outcomes. Literature results confirm better preservation of renal function, with safety outcomes comparable to those with clamping of the main renal artery [6–8]. When selective clamping is planned on the basis of standard bidimensional images, the approach can be confirmed intraoperatively with indocyanine green (ICG) injection [9–11]. However, even under ICG guidance, selective clamping remains a critical step in NSS owing to the potential risk of bleeding if an incorrect vascular management strategy is used [12,13]. The introduction of hyperaccuracy three-dimensional virtual models (3DVMs) partly solved this issue by increasing understanding of the vascular anatomy during planning and aiding the surgeon intraoperatively via direct overlay of images on the operative field through augmented reality (AR) technology [14–17]. However, this technology may not be sufficient to guarantee an appropriate avascular resection plane, and the surgeon may have to switch to global clamping. Intraoperative failure might be because of the empirical definition of vascular boundaries within the kidney given by the 3DVMs, based only on the direction of the arterial branches entering the renal sinus rather than perfused regions.

The primary aim of this study was to assess the reliability of new-generation 3DVMs of the kidney that reproduce the different perfusion regions instead of empirically estimating them. The second aim was to evaluate the role of these models in helping the surgeon to perform safe and effective selective clamping during surgery and their impact on postoperative renal function.

2. Patients and methods

2.1. Study population

We prospectively enrolled all consecutive patients with a radiological diagnosis of an organ-confined single renal mass who underwent robot-assisted partial nephrectomy (RAPN) with intraoperative image guidance at our center from January 2021 to May 2022. The study was conducted in accordance with good clinical practice guidelines, and informed consent was obtained from the patients. According to Italian law (Agenzia Italiana del Farmaco guidelines for observational studies, March 20, 2008), no formal institutional review board or ethics committee approval was needed.

All patients underwent abdominal four-phase contrast-enhanced computed tomography (CT) within 3 mo before surgery. Exclusion criteria were evidence of anatomic abnormalities, such as a horseshoe-shaped or ectopic kidney. Patients with preoperative imaging that was inadequate for creating a 3DVM (such as those with CT images with a slice acquisition interval of >3 mm or suboptimal difference of enhancement among the phases) and patients with imaging older than 3 mo were also excluded.

2.2. 3DVM production

Multiphase CT images in DICOM format were processed by Medics (www.medics3d.com, Turin, Italy) using a dedicated process for hyperaccuracy 3D (HA3D) reconstruction of patient-specific clinical cases. The kidney, tumor, arterial and venous branches, and the collecting system were segmented using specific algorithms and software for final production of a 3DVM as previously described [15].

To estimate the kidney perfusion regions, a Voronoi diagram, a mathematical tool based on Euclidean distances, was applied to the 3DVMs to calculate the vascular-dominant regions [18].

The HA3D perfusion regions were calculated by subdividing the healthy parenchyma into anatomic volumes according to the morphology and proximity of each arterial branch and considering the intrasinusal portion of the segmentary vessels up to 1 cm from the interface between each vessel and the parenchymal tissue. From the artery model, a center line was extracted using validated vascular modeling toolkit (VMTK) libraries [19]. To adapt the 3DVM for the algorithm, the center line for each arterial branch was represented as a set of seed points lying on consecutive bidimensional planes (Fig. 1A). Each organ parenchyma voxel was then associated with a center-line point (ie, a seed) according to a proximity criterion. For each voxel of the kidney, the closest Euclidian distance from a seed point of the arterial center line was calculated. The algorithm assigned each single voxel to a specific arterial branch with the highest probability of supplying that voxel, thus defining a specific perfusion area (Fig.1B). The algorithm combined all the data for each bidimensional plane and its relative center line points consecutively to produce a 3DVM of the parenchyma composed of distinct regions of vascularization, each rendered in a specific color for clear distinguishability from the others (Fig. 1C, D). The final output was in STL format. The bioengineer uploaded the file to an ICON platform [20] for planning of the surgical strategy and guidance during the procedure.

2.3. 3DVM-assisted surgery

All the surgeries were performed robotically by the same expert surgeon (>1000 procedures carried out) via a transperitoneal approach. Before each procedure, the surgeon assessed the 3DVMs via the ICON platform

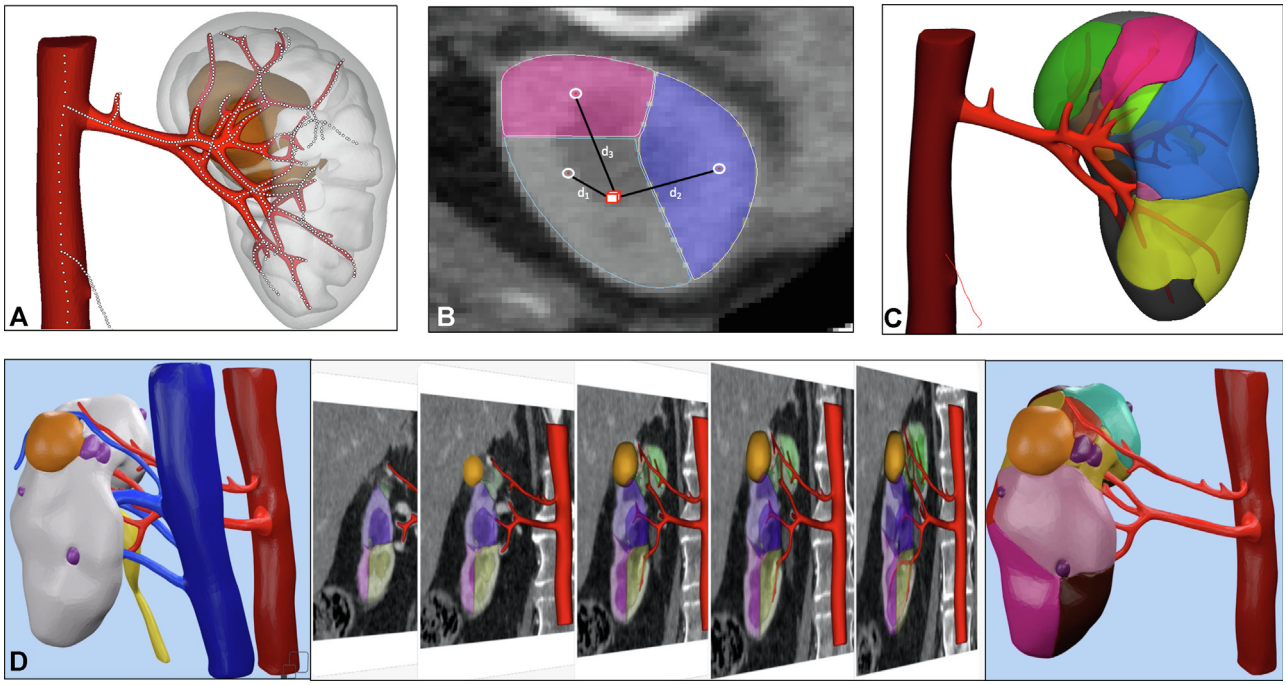

Fig. 1 – Different phases in the production of a perfusion-region three-dimensional virtual model (3DVM) with software using a Voronoi diagram. (A) From an artery model visualization of the arterial phase of a computed tomography scan, a center line is extracted and represented as a set of seed points laid on consecutive bidimensional planes to adapt the 3DVM to the algorithm. (B) Each kidney parenchyma voxel is associated with a center-line point (ie, a seed) according to a proximity criterion using the mathematical Euclidian distance from a seed point of the arterial center line to define each perfusion area. (C) The final product computed by the algorithm with all the data for each bidimensional plane and its relative center-line points and areas, which are combined consecutively to create a 3DVM of the parenchyma with distinct regions of vascularization, each rendered in a specific color. (D) Representation of the entire production process for the 3DVM, starting from the standard model to the new generation that includes a representation of the perfusion areas.

[20] to plan the surgical strategy. For the purpose of the study, he was asked to define the renal pedicle management in advance after looking at the perfusion regions of the virtual model, and to document the number and level/order of arterial branches to be clamped in a possible attempt at selective clamping. The surgeon considered the tumor location in the kidney in relation to the vascular perfusion regions in contact with its surface and planned clamping of the vessels feeding those regions to achieve a bloodless resection field limited to the peritumoral tissue as much as possible.

The surgical procedure was performed under intraoperative 3DVM assistance, in both a cognitive and an AR fashion, using the Tile-pro technology of the da Vinci robotic platform as previously described [21].

During the intervention, the renal pedicle was managed according to the principles set in the planning phase, ranging from clampless or selective clamping to a global clamping strategy. After kidney exposure, the main renal artery was identified and dissected, with isolation of the segmental branches entering the renal sinus and any accessory and aberrant arteries identified by the 3DVM. Once the renal pedicle was dissected, the renal mass was exposed or marked on the kidney surface (if totally endophytic) under AR guidance and US confirmation.

The arteries preoperatively identified under 3DVM assistance as those feeding the perfusion areas close to the renal mass were clamped with bulldog clips for selective clamping. When global ischemia was planned, the main artery was clamped, while no clamping was performed when a clampless procedure was planned.

In cases managed with selective clamping, near-infrared fluorescence was used to confirm the correct vascular management. A solution of ICG (0.1–0.5 mg/ml/kg) was intravenously injected for visualization of the portions of the kidney still receiving blood flow as bright green areas, with clamped areas appearing as grey, and precise identification of the boundaries and shapes of the different perfusion regions in the kidney (Fig. 2).

2.4. Measurements

For each patient, we prospectively collected demographic data including age, body mass index; comorbidities classified according to the Charlson comorbidity index (CCI) [22]; clinical tumor size, side, location, and complexity according to the PADUA score [23]; perioperative data (including management of the renal pedicle, type and duration of ischemia); pathological data (including TNM stage [24]); and postoperative complications classified according to the Clavien-Dindo scheme [25]. In terms of functional assessments, serum creatinine and the estimated glomerular filtration rate (eGFR) were measured preoperatively and 3 mo after surgery. Split renal function (SRF) and estimated renal plasmatic flow (ERPF) were evaluated using ^{99m}Tc-mercaptoacetyltriglycine renal scintigraphy at the same time points. The baseline-weighted differential was calculated as a measure of the percentage reduction in SRF and ERPF from baseline.

The total number of perfusion regions was recorded after evaluation of each 3DVM, and the location of each renal mass was evaluated in relation to the number of perfusion regions it crossed.

2.5. Statistical analysis

The sample size was calculated using the *pwr* package in R v4.2.1, considering a small effect size (d = 0.25) and expected power of 80%. The number of patients for recruitment to meet these criteria was 99 in total. Patient characteristics were compared using Fisher's exact test for cate-

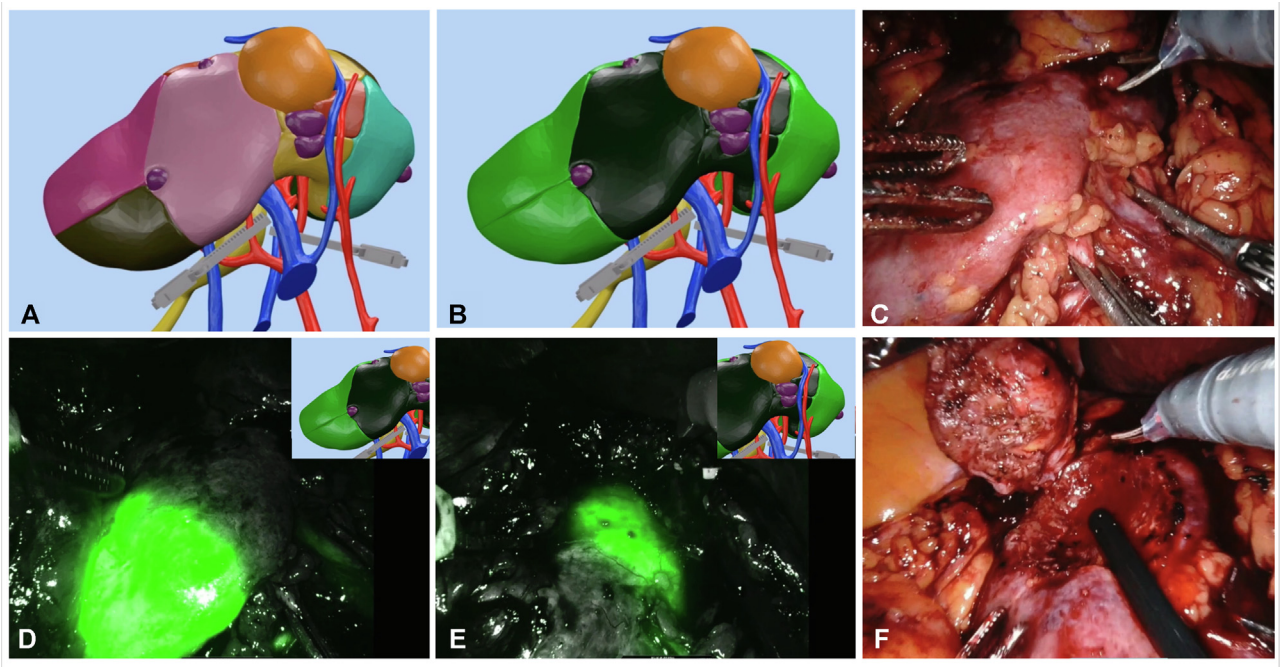

Fig. 2 – Planning and intraoperative confirmation of a selective clamping strategy during robot-assisted right partial nephrectomy. (A) Virtual simulation of selective clamping on the basis of the perfusion-region three-dimensional virtual model. (B) Virtual simulation of the ischemic region and of areas retaining vascularization. (C) Intraoperative management of the arterial branches following the preoperatively planned clamping strategy. (D,E) Intraoperative confirmation via indocyanine green injection of the accuracy of the selective clamping, with blood flow maintained at the upper and lower poles of the kidney. (F) Final steps of the enucleation, showing a bloodless field at the level of the resection bed.

gorical variables and the Mann-Whitney test for continuous variables. Results are expressed as the median (interquartile range [IQR]) or mean (standard deviation [SD]) for continuous variables, and as the frequency and proportion for categorical variables. Baseline and postoperative functional data (serum creatinine, eGFR, SRF and ERPF) were compared using paired-sample t tests. Data were analyzed using Jamovi v.2.3.

3. Results

A total of 103 patients underwent 3DVM-assisted RAPN during the enrollment phase. Patient demographics and preoperative characteristics are reported in Table 1. The median age was 66 yr. The median body mass index was 25.8 kg/m2 (IQR 23.4–28.6) and the median CCI was 2 (IQR 2–3). The median tumor size was 36 mm (IQR 25–48) and the median PADUA score was 8 (IQR 7–9). Of the 103 renal masses considered, 41.7% were classified as low-complexity, 39.8% as intermediate-complexity, and 18.5% s high-complexity.

As reported in Table 2, 44 patients underwent 3DVM-assisted RAPN under AR guidance, while intraoperative assistance was cognitive for 59 patients.

The vascular pedicle was managed with selective clamping in 79 patients (76.7%) and main artery clamping in 16 (15.5%), while eight patients (7.8%) had a clampless procedure. A significant difference in the distribution of patients treated with global clamping, selective clamping, or clampless approach stratified by PADUA risk category ($p = 0.001$), with a progressive increase in the use of global clamping from low to high tumor complexity (9.3% for category 1, 12.2% for category 2, and 36.8% for category 3), with

Table 1 – Characteristics of the study population ($n = 103$)

Parameter	Result
Median age, yr (IQR)	66 (57–74)
Median body mass index, kg/m^2 (IQR)	25.8 (23.4–28.6)
Median CCI (IQR)	2 (2–3)
ASA score, *n* (%)	
≤2	82 (79.6)
>2	21 (20.3)
Median CT lesion size, mm (IQR)	36 (25–48)
Clinical stage, *n* (%)	
cT1a	65 (63.1)
cT1b	34 (33)
cT2	4 (3.9)
Kidney face location, *n* (%)	
Anterior face	49 (47.6)
Posterior face	54 (52.4)
Tumor side, *n* (%)	
Right	49 (47.6)
Left	54 (52.4)
Tumor location, *n* (%)	
Upper pole	29 (28.1)
Mesorenal	45 (43.8)
Lower pole	29 (28.1)
Tumor growth pattern, *n* (%)	
>50% exophytic	57 (55.3)
<50% exophytic	31 (30.1)
Endophytic	15 (14.6)
Kidney rim location, *n* (%)	
Lateral margin	59 (57.2)
Medial margin	44 (42.8)
Median PADUA score (IQR)	8 (7–9)
PADUA risk category, *n* (%)	
Category 1 (PADUA <8)	43 (41.7)
Category 2 (PADUA 8–9)	41 (39.8)
Category 3 (PADUA ≥10)	19 (18.5)

ASA = American Society of Anesthesiologists; CCI = Charlson comorbidity index; CT = computed tomography; IQR = interquartile range.

Table 2 – Perioperative variables for the 103 patients undergoing robot-assisted partial nephrectomy guided by a perfusion-region three-dimensional virtual model

Parameter	Result
Augmented reality procedure, *n* (%)	44 (42.7)
Median operative time, min (IQR)	92 (75–110)
Hilar clamping, *n* (%)	
Clampless	8 (7.8)
Global clamping	16 (15.5)
Selective clamping	79 (76.7)
Hilar clamping by PADUA risk category, *n* (%)*	
Category 1 (*n* = 43, 41.7%)	
Clampless	8 (18.6)
Global clamping	4 (9.3)
Selective clamping	31 (72.1)
Category 2 (*n* = 41, 39.8%)	
Clampless	0 (0)
Global clamping	5 (12.2)
Selective clamping	36 (87.8)
Category 3 (*n* = 19, 18.5%)	
Clampless	0 (0)
Global clamping	7 (36.8)
Selective clamping	12 (63.2)
Median ischemia time, min (IQR)	
Global ischemia	17 (15–25)
Selective ischemia	16 (12–20)
Median EBL, cm^3 (IQR)	180 (100–300)
Extirpative technique, *n* (%)	
Pure enucleation	67 (65)
Enucleoresection	36 (35)
Opening of the collecting system, *n* (%)	
Yes	20 (19.4)
No	83 (80.6)
Intraoperative complications, *n* (%)	1 (1.9)
Postoperative complications, *n* (%)	11 (10.6)
Postoperative CD grade >2 complications, *n* (%)	2 (1.9)
Median LOS, d (IQR)	5 (4–6)

CD = Clavien-Dindo; EBL = estimated blood loss; LOS = length of stay; IQR = interquartile range.
* *p* = 0.001 for distribution of the clamping approach by PADUA category.

Table 3 – Perfusional kidney and tumor characteristics for the 103 patients

Parameter	Result		*p* value
Median kidney perfusion regions, *n* (IQR)	8 (7–10)		
Median tumor perfusion regions, *n* (IQR)	3 (2–3)		
Tumor perfusion regions, *n* (%)			
1 region	14 (13.6)		
2 regions	36 (34.9)		
3 regions	34 (33.0)		
4 regions	14 (13.6)		
5 regions	5 (4.9)		
	3DVM POP	**3DVM IOM**	
Clamped arteries, *n* (%)			0.12
0 arteries	8 (7.8)	8 (7.8)	
1 artery	53 (51.5)	68 (66.0)	
2 arteries	36 (34.9)	25 (24.3)	
≥3 arteries	6 (5.8)	2 (1.9)	
Clamped artery order, *n* (%)			0.71
Clampless	8 (7.8)	8 (7.8)	
First-order artery	12 (11.6)	16 (15.5)	
Second-order artery	41 (39.8)	44 (42.7)	
Third-order artery	42 (40.8)	35 (34.0)	
Perfusion regions under ischemia, *n* (%)			0.18
Lower number than TPRs	8 (7.8)	16 (15.5)	
Same number as TPRs	48 (46.6)	36 (35.0)	
Higher number than TPRs	35 (34.0)	35 (34.0)	
All kidney perfusion regions	12 (11.6)	16 (15.5)	

3DVM = three-dimensional virtual model; IOM = intraoperative management; IQR = interquartile range; POp = preoperative planning; TPRs = tumor perfusion regions.

extensive use of selective clamping for intermediate-complexity kidneys (87.8%). The clampless approach was only used for low-complexity tumors.

The median ischemia time was 17 min (IQR 15–25) for global clamping and 16 min (IQR 12–20) for selective clamping. Pure enucleation was performed in 67 cases (65%) and violation of the collecting system was recorded for 19.4% of the surgeries.

The mean operative time was 93.8 min (SD 27.6) and the mean EBL was 211 ml (SD 132), with no differences observed by hilar clamping strategy.

Only one intraoperative complication (0.9%; focal violation of an arterial aneurysm at the level of the retropyelic artery, managed intraoperatively with a dedicated stitch) was recorded and no conversions to radical nephrectomy occurred. Overall, the postoperative complication rate was 10.6% (11/103), with a Clavien grade >2 complication rate of 1.9%.

The kidney perfusion features and tumor characteristics of the cohort, as assessed using the 3DVMs, are reported in Table 3.

The median number of perfusion regions per kidney was 8 (IQR 7–10). The PR-3DVMs revealed the following distribution of perfused regions crossing the tumor: 13.6%, one region; 34.9%, two regions; 33%, three regions; 13.6%, four regions; and 4.9%, five regions.

Comparison of the distribution of patients by the number and order of arteries clamped according to the preoperative plan and actual intraoperative evidence revealed no significant differences for the number ($p = 0.12$) or order ($p = 0.71$) of the arteries clamped.

Regarding the number of perfusion regions in contact with the tumor that were under ischemia during surgery, for 50.5% of the cases their number was the same of the planning or even lower; for 34.0% was higher, but the same that was planned preoperatively. Only 3.9% of the cases (4/103) needed an intraoperative switch from selective to global clamping, with a 15.5% cumulative rate of ischemia to all the perfusion regions of the kidney. Among the four cases in which management of the renal pedicle changed during surgery, the tumor (intermediate complexity) was located at the lateral margin of the kidney, close to the vascular regions fed by the retropyelic artery in two. During the planning phase, the surgeon proposed selective clamping of the prepyelic branches only, but non-negligible bleeding from the posterior portion of the resection bed during surgery prompted a switch in strategy to clamping of the retropyelic artery as well. The third case was a low-complexity polar tumor scheduled for superselective clamping but managed with a clampless approach. The last case was a highly complex, totally endophytic tumor for which an enucleative strategy was planned, with sparing of a small portion of the lower pole of the kidney for which

vascularization should have been maintained during surgery. The case was managed with a hemi-nephrectomy, with removal of the lower pole together with the tumor, and therefore its blood flow was interrupted.

Pathological and functional data are reported in Table 4. Two (1.9%) positive surgical margins were recorded. There were no differences in functional outcomes (mean serum creatinine and eGFR) between baseline and 3-mo follow-up for either the whole cohort ($p = 0.34$ and $p = 0.11$) or after stratification by clamped artery order ($p = 0.76$).

Functional results for the group of 51 patients who underwent baseline and 3-mo renal scintigraphy are reported in Supplementary Table 1.

The changes in SRF and ERPF for the operated kidney differed significantly by clamping strategy. The mean decrease in SRF was 11.3% for global clamping versus 7.7% for selective clamping (first-order artery) and 1.7% for superselective (second-order artery) clamping ($p = 0.004$). The mean decrease in ERPF was 18.9% for global clamping versus 9.9% for selective clamping and 6.0% for superselective clamping ($p = 0.02$). None of the patients in this subgroup underwent clampless surgery.

Table 4 – Postoperative and functional variables for the 103 patients

Parameter	Result		*p* value
Pathological stage, *n* (%)			
Benign	24 (23.3)		
pT1a	47 (45.6)		
pT1b	22 (21.3)		
pT2	4 (3.9)		
pT3a	6 (5.9)		
Median pathological tumor size, mm (IQR)	34 (25–48)		
Positive surgical margin, *n* (%)	2 (1.9)		
ISUP grade, *n* (%)			
Grade1	22 (21.5)		
Grade 2	35 (33.9)		
Grade 3	13 (12.6)		
Not applicable	33 (32)		
Median SCr, mg/dl (IQR)			0.34
Baseline	0.92 (0.78–1.07)		
Postoperative	0.99 (0.81–1.20)		
Median change in SCr, % (IQR)	5.9 (−3.60 to 19.1)		
Median eGFR, ml/min/1.73 m^2 (IQR)			0.11
Baseline	82.8 (63.25–98.75)		
Postoperative	70.0 (55.25–88.75)		
Median change in eGFR, % (IQR)	9.1 (0.01–22.1)		
	Baseline	**Postoperative**	
Mean SCr, mg/dl (SD)			0.76
Clampless	1.02 (0.20)	1.08 (0.22)	
Global clamping	0.90 (0.21)	1.04 (0.36)	
Selective clamping (second-order)	(0.54)	1.15 (0.74)	
Selective clamping (third-order)	0.98 (0.33)	1.19 (0.50)	
Mean eGFR, ml/min/1.73 m^2 (SD)			0.33
Clampless	83.2 (19.4)	80.5 (25.6)	
Global clamping	82.2 (21)	69.3 (22.4)	
Selective clamping (second-order)	83.4 (30.7)	75.6 (32)	
Selective clamping (third-order)	75.9 (22)	69.2 (22.8)	

ISUP = International Society of Urological Pathology; eGFR = estimated glomerular filtration rate; SCr = serum creatinine; EBL = estimated blood loss; RCC = renal cell carcinoma; IQR = interquartile range; SD = standard deviation.

4. Discussion

We previously evaluated the role of 3DVMs during RAPN and demonstrated that this technology is helpful in avoiding global ischemia of the healthy renal remnant and minimizing postoperative functional loss [15,26,27]. However, management of the vascular pedicle, even when planned with 3DVMs, has remained somewhat empirical to date, with a need for intraoperative variation of the clamping strategy in cases of unforeseen bleeding from the resection remnant [28].

This evidence is in line with some anatomic studies that demonstrated that the renal arterial vasculature cannot be schematized according to the classic Graves classification because of wide variability in the distribution of the arterial branches [29–31]. Moreover, as reported by Macchi et al. [31], another variable to consider is the presence of a collateral arterial blood supply between different renal segments that differs from the classic anatomic knowledge based on the idea of a terminal supply for each segmental artery [31].

Considering these issues, we developed a new generation of 3DVMs for which a mathematical algorithm is used to visualize the perfusion regions for each segmental artery entering the renal parenchyma. We tested the accuracy of the new models in defining each perfusion region in comparison to real intraoperative evidence and thus their efficacy in achieving precise selective clamping and devascularization of the perilesional parenchymal volume. Our results highlight some crucial points of discussion.

First, from an anatomic perspective, the PR-3DVMs demonstrated non-negligible variability in the number of vascular regions fed by each segmental artery. Among the 103 cases, the median number of perfusion regions was eight and ranged from four to 13 across the cohort.

The number of perfusion regions in contact with the tumor was also highly variable: 48.5% of the virtual reconstructions showed one or two perfusion regions in contact with the lesion surface, while tumors were perfused by three regions in 33% and by four or more regions in 18.5% of cases.

This information was fundamental in choosing the correct clamping strategy, allowing the surgeon to plan the number and order of arteries to be clamped for effective devascularization of the peritumoral parenchymal tissue. The number of selective clamping procedures performed under PR-3DVM guidance was thus very high (76.7%), with extensive use in the subgroups of patients with intermediate-complexity (87.8%) and high-complexity (63.2%) tumors.

In terms of the number of arteries clamped, intraoperative management mainly involved clamping of a single arterial vessel (66%), but one in four cases required clamping of two different segmental arteries to gain a bloodless field during tumor resection.

Regarding the order of the arteries clamped during surgery, the majority of cases were managed with second-order artery clamping (42.7%), although a significant number of patients (34%) also underwent third-order artery clamping.

Of main interest regarding the efficacy of the new PR-3DVMs in allowing safe selective clamping, there were no differences in operative time, EBL or PSM in comparison to global clamping.

Moreover, comparison between the preoperative plan and actual intraoperative management of the vascular pedicle did not reveal a significant difference in either the number (p = 0.12) or order (p = 0.71) of the arteries that were clamped.

Another point of evidence confirming previous data comes from evaluation of the perfusion regions that underwent ischemia. We limited ischemia exactly to regions in contact with the tumor in one-third of the patients, minimizing functional injury to the kidney. In a further one-third of the patients, selective clamping involved a higher number of perfusion regions than those in contact with the tumor, but vascularization was maintained in areas of the kidney far from the lesion. This case-by-case approach allowed us to plan selective or superselective clamping before surgery. Comparison of the preoperative plan and the intraoperative surgical evidence revealed high concordance. This rational approach allowed the surgeon to avoid ischemia to a large number of kidney regions, with a global clamping rate of only 15.5% and a low rate of intraoperative switching from selective to global clamping (3.9%).

Successful translation to clinical practice of the new anatomic insights provided by this tool is confirmed by the functional results obtained via renal scintigraphy (Supplementary Table 1). Results for the 51 patients who underwent scintigraphy at baseline and 3 mo demonstrate the significant functional advantages for the operated kidney in terms of SRF (p = 0.004) and ERPF (p = 0.02) when selective or superselective clamping was used. This confirms that limiting ischemic regions reduces the impairment of postoperative renal function.

Our study has limitations related to the technology itself and to the study design. First, a bioengineer expert in uro-oncology is needed to manually refine the 3D model segmentation of the kidneys. Second, concordance between the virtual and real regions identified on ICG injection was evaluated for each case according to visual assessment by the surgeon, which lacks objective metrics. Third, there are some limits to adoption of these new PR-3DVMs in daily practice, mainly related to the costs associated with their production and use with the dedicated ICON platform.

Moreover, a single surgeon with high experience in minimally invasive renal surgery and vascular pedicle manipulation performed all the procedures in the study, potentially limiting the reproducibility of the perioperative outcomes reported here. Similarly, the study was conducted in a single center experienced in the use of 3DVM-guided surgery, further limiting the reproducibility. Finally, the lack of randomization to a control group in which cognitive clamping was performed limits the strength of our results.

Notwithstanding the limitations, use of this tool in the intraoperative setting allowed the surgeon to follow the planned strategy step-by-step by consulting the PR-3DVM to perform precise selective clamping (correlation of 96.1% between planning and intraoperative evidence) and proper focus on the tumor resection and suture phases without the stress of worrying about global ischemia time.

The development of this new generation of 3DVMs changes the perspective for surgical management in PN by providing a high level of accuracy for selective clamping in precision surgery [32].

5. Conclusions

This study demonstrates the accuracy and efficacy of a new 3DVM of the kidney for which a mathematical algorithm is used to split the parenchymal volume into its vascular perfusion regions during digital production. The information given by this innovative tool significantly contributes to current knowledge of anatomic principles of the kidney vasculature and can help surgeons in performing a super-tailored nephron-sparing procedure to minimize the extent of ischemia and functional impairment with the highest level of safety possible.

Author contributions: Daniele Amparore had full access to all the data in the study and takes responsibility for the integrity of the data and the accuracy of the data analysis.

Study concept and design: Amparore, Porpiglia.
Acquisition of data: Amparore, Piramide, Checcucci, Verri, De Cillis, Piana, Volpi, Busacca, Colombo.
Analysis and interpretation of data: Amparore, Piramide, Checcucci.
Drafting of the manuscript: Amparore, Piramide, Checcucci, Verri.
Critical revision of the manuscript for important intellectual content: Amparore, Piramide, Fiori, Porpiglia.
Statistical analysis: Piramide.
Obtaining funding: None.
Administrative, technical, or material support: None.
Supervision: Fiori, Porpiglia.
Other: None.

Financial disclosures: Daniele Amparore certifies that all conflicts of interest, including specific financial interests and relationships and affiliations relevant to the subject matter or materials discussed in the manuscript (eg, employment/affiliation, grants or funding, consultancies, honoraria, stock ownership or options, expert testimony, royalties, or patents filed, received, or pending), are the following: None.

Funding/Support and role of the sponsor: None.

Supplementary data

A Peer Review Summary, Supplementary data and The Surgery in Motion video accompanying this article can be found in the online version at https://doi.org/10.1016/j.eururo.2023.04.005 and via www.europeanurology.com.

References

[1] Shao P, Tang L, Li P, et al. Application of a vasculature model and standardization of the renal hilar approach in laparoscopic partial nephrectomy for precise segmental artery clamping. Eur Urol 2013;63:1072–81. https://doi.org/10.1016/j.eururo.2012.10.017.

[2] Gill IS, Eisenberg MS, Aron M, et al. "Zero ischemia" partial nephrectomy: novel laparoscopic and robotic technique. Eur Urol 2011;59:128–34. https://doi.org/10.1016/j.eururo.2010.10.002.

[3] Ng CK, Gill IS, Patil MB, et al. Anatomic renal artery branch microdissection to facilitate zero-ischemia partial nephrectomy. Eur Urol 2012;61:67–74. https://doi.org/10.1016/j.eururo.2011.08.040.

[4] Qian J, Li P, Qin C, et al. Laparoscopic partial nephrectomy with precise segmental renal artery clamping for clinical T1b tumors. J Endourol 2015;29:1386–91. https://doi.org/10.1089/end.2015.0359.

[5] Gill IS, Patil MB, de Castro Abreu AL, et al. Zero ischemia anatomical partial nephrectomy: a novel approach. J Urol 2012;187:807–14. https://doi.org/10.1016/j.juro.2011.10.146.

[6] Martin GL, Warner JN, Nateras RN, Andrews PE, Humphreys MR, Castle EP. Comparison of total, selective, and nonarterial clamping techniques during laparoscopic and robot-assisted partial nephrectomy. J Endourol 2012;26:152–6. https://doi.org/10.1089/end.2011.0304.

[7] Zhang L, Wu B, Zha Z, Zhao H, Yuan J, Jiang Y. Comparison of selective and main renal artery clamping in partial nephrectomy of renal cell cancer: a PRISMA-compliant systematic review and meta-analysis. Medicine 2018;97:e11856. https://doi.org/10.1097/MD.0000000000011856.

[8] Mattevi D, Luciani LG, Mantovani W, et al. Fluorescence-guided selective arterial clamping during RAPN provides better early functional outcomes based on renal scan compared to standard clamping. J Robot Surg 2019;13:391–6. https://doi.org/10.1007/s11701-018-0862-x.

[9] Bjurlin MA, Gan M, McClintock TR, et al. Near-infrared fluorescence imaging: emerging applications in robotic upper urinary tract surgery. Eur Urol 2014;65:793–801. https://doi.org/10.1016/j.eururo.2013.09.023.

[10] Diana P, Buffi NM, Lughezzani G, et al. The role of intraoperative indocyanine green in robot-assisted partial nephrectomy: results from a large, multi-institutional series. Eur Urol 2020;78:743–9. https://doi.org/10.1016/j.eururo.2020.05.040.

[11] Veccia A, Antonelli A, Hampton LJ, et al. Near-infrared fluorescence imaging with indocyanine green in robot-assisted partial nephrectomy: pooled analysis of comparative studies. Eur Urol Focus 2020;6:505–12. https://doi.org/10.1016/j.euf.2019.03.005.

[12] Borofsky MS, Gill IS, Hemal AK, et al. Near-infrared fluorescence imaging to facilitate super-selective arterial clamping during zero-ischaemia robotic partial nephrectomy. BJU Int 2013;111:604–10. https://doi.org/10.1111/j.1464-410X.2012.11490.x.

[13] Harke N, Schoen G, Schiefelbein F, Heinrich E. Selective clamping under the usage of near-infrared fluorescence imaging with indocyanine green in robot-assisted partial nephrectomy: a single-surgeon matched-pair study. World J Urol 2014;32:1259–65. https://doi.org/10.1007/s00345-013-1202-4.

[14] Shirk JD, Thiel DD, Wallen EM, et al. Effect of 3-dimensional virtual reality models for surgical planning of robotic-assisted partial nephrectomy on surgical outcomes: a randomized clinical trial. JAMA Netw Open 2019;2:e1911598. https://doi.org/10.1001/jamanetworkopen.2019.11598.

[15] Porpiglia F, Fiori C, Checcucci E, Amparore D, Bertolo R. Hyperaccuracy three-dimensional reconstruction is able to maximize the efficacy of selective clamping during robot-assisted partial nephrectomy for complex renal masses. Eur Urol 2018;74:651–60. https://doi.org/10.1016/j.eururo.2017.12.027.

[16] Maddox MM, Feibus A, Liu J, Wang J, Thomas R, Silberstein JL. 3D-printed soft-tissue physical models of renal malignancies for individualized surgical simulation: a feasibility study. J Robot Surg 2018;12:27–33. https://doi.org/10.1007/s11701-017-0680-6.

[17] Wake N, Bjurlin MA, Rostami P, Chandarana H, Huang WC. Three-dimensional printing and augmented reality: enhanced precision for robotic assisted partial nephrectomy. Urology 2018;116:227–8. https://doi.org/10.1016/j.urology.2017.12.038.

[18] Wang C, Roth HR, Kitasaka T, et al. Precise estimation of renal vascular dominant regions using spatially aware fully convolutional networks, tensor-cut and Voronoi diagrams. Comput Med Imaging Graph 2019;77:101642. https://doi.org/10.1016/j.compmedimag.2019.101642.

[19] Antiga L, Piccinelli M, Botti L, Ene-Iordache B, Remuzzi A, Steinman DA. An image-based modeling framework for patient-specific computational hemodynamics. Med Biol Eng Comput 2008;46:1097–112. https://doi.org/10.1007/s11517-008-0420-1.

[20] Ruzzenente A, Alaimo L, Conci S, et al. Hyper accuracy three-dimensional (HA3D™) technology for planning complex liver resections: a preliminary single center experience. Updates Surg 2023;75:105–14. https://doi.org/10.1007/s13304-022-01365-8.

[21] Porpiglia F, Checcucci E, Amparore D, et al. Three-dimensional augmented reality robot-assisted partial nephrectomy in case of complex tumours (PADUA ≥10): a new intraoperative tool overcoming the ultrasound guidance. Eur Urol 2020;78:229–38. https://doi.org/10.1016/j.eururo.2019.11.024.

[22] Nuttall M, van der Meulen J, Emberton M. Charlson scores based on ICD-10 administrative data were valid in assessing comorbidity in patients undergoing urological cancer surgery. J Clin Epidemiol 2006;59:265–73. https://doi.org/10.1016/j.jclinepi.2005.07.015.

[23] Ficarra V, Novara G, Secco S, et al. Preoperative aspects and dimensions used for an anatomical (PADUA) classification of renal tumours in patients who are candidates for nephron-sparing surgery. Eur Urol 2009;56:786–93. https://doi.org/10.1016/j.eururo.2009.07.040.

[24] Ljungberg B, Albiges L, Abu-Ghanem Y, et al. European Association of Urology guidelines on renal cell carcinoma: limited update March 2021. Eur Urol 2021;75:799–810. https://doi.org/10.1016/j.eururo.2019.02.011.

[25] Dindo D, Demartines N, Clavien P-A. Classification of surgical complications: a new proposal with evaluation in a cohort of 6336 patients and results of a survey. Ann Surg 2004;240:205–13.

[26] Amparore D, Pecoraro A, Checcucci E, et al. Three-dimensional virtual models' assistance during minimally invasive partial nephrectomy minimizes the impairment of kidney function. Eur Urol Oncol 2022;5:104–8. https://doi.org/10.1016/j.euo.2021.04.001.

[27] Piramide F, Kowalewski K-F, Cacciamani G, et al. Three-dimensional model–assisted minimally invasive partial nephrectomy: a systematic review with meta-analysis of comparative studies. Eur Urol Oncol 2022;5:640–50. https://doi.org/10.1016/j.euo.2022.09.003.

[28] Badani KK, Kothari PD, Okhawere KE, et al. Selective clamping during robot-assisted partial nephrectomy in patients with a solitary kidney: is it safe and does it help? BJU Int 2020;125:893–7. https://doi.org/10.1111/bju.15043.

[29] Weld KJ, Bhayani SB, Belani J, Ames CD, Hruby G, Landman J. Extrarenal vascular anatomy of kidney: assessment of variations and their relevance to partial nephrectomy. Urology 2005;66:985–9. https://doi.org/10.1016/j.urology.2005.05.023.

[30] Kang WY, Sung DJ, Park BJ, et al. Perihilar branching patterns of renal artery and extrarenal length of arterial branches and tumour-feeding arteries on multidetector CT angiography. Br J Radiol 2013;86:20120387. https://doi.org/10.1259/bjr.20120387.

[31] Macchi V, Crestani A, Porzionato A, et al. Anatomical study of renal arterial vasculature and its potential impact on partial nephrectomy. BJU Int 2017;120:83–91. https://doi.org/10.1111/bju.13788.

[32] Autorino R, Porpiglia F, Dasgupta P, et al. Precision surgery and genitourinary cancers. Eur J Surg Oncol 2017;43:893–908. https://doi.org/10.1016/j.ejso.2017.02.005.